Application of the finite-size Lyapunov exponent to particle tracking velocimetry in fluid mechanics experiments

Natalie Kleinfelter,[1] Monica Moroni,[2] and John H. Cushman[3,*]
[1]*Department of Mathematics, Purdue University, West Lafayette, Indiana 47907, USA*
[2]*Department of Hydraulics, Transportations and Roads, University of Rome "La Sapienza," Rome, Italy*
[3]*Department of Earth and Atmospheric Sciences and Department of Mathematics, Purdue University, West Lafayette, Indiana 47907, USA*
(Received 9 February 2005; published 2 November 2005)

A finite-size (or scale) Lyapunov exponent (FSLE), $\lambda_a(x)$, is presented in a statistical mechanical framework and employed to characterize mixing in a variety of laboratory and computational fluid mechanics experiments. The FSLE is the exponential rate at which two particles separate from a distance x to ax. Laboratory particle tracking experiments are used to study penetrative convection and flow in porous media while computational experiments are used to study Lévy processes and deterministic diffusion. The apparent scaling relation $\lambda_a(x) \sim C_a x^{-\beta(a)}$ of the FSLE holds over intermediate initial separations where the laboratory experiment data is most accurate and asymptotically for the computational experiments. The dependence of the exponent β on a decreases with increasing a. In the matched index porous system, C_a is also a function of mean fluid velocity. The exponent β is α when the Lévy process is α-stable and in this case β is independent of a.

DOI: 10.1103/PhysRevE.72.056306 PACS number(s): 47.90.+a, 05.20.−y, 92.10.Lq

I. INTRODUCTION

Velocity fluctuations over a hierarchy of space-time scales drive dispersive mixing in fluids. Pressure differences, heterogeneity in porous media, viscosity, buoyancy, and temperature differences all lead to dispersive mixing. This article is focused on examining the mixing process for a variety of flow fields by employing the finite-size (or scale) Lyapunov exponent (FSLE) as well as introducing a statistical mechanical definition for the FSLE. All experiments reported herein are designed to capture the trajectories of labeled particles. These trajectories are used to construct the FSLE,

$$\lambda_a(x) = \frac{1}{T_a(x)} \ln a,$$

a measure of the growth rate of the mixing zone, or alternatively, a measure of the growth rate of finite-size perturbations. Here $T_a(x)$, the a-time, is the average time it takes two particles separated by a distance x to reach a separation of ax. Since ax is the threshold, a is called the threshold ratio. If x is thought of as a measure of the scale of the mixing layer in a dispersive flow, then $\lambda_a(x)$ measures the exponential rate of growth to scale ax,

$$e^{\lambda_a(x) T_a(x)} = a.$$

A heuristic definition of λ_a was presented in Aurell *et al.* [1,2] and several of its properties were studied in the context of Shannon's information theory. In the Fickian limit, Aurell *et al.* showed the FSLE will be inversely proportional to the square of the initial separation and directly proportional to the classical diffusion coefficient [2].

The FSLE may be used in a Lagrangian setting to study dispersive mixing at different scales. It is a generalization to finite separations of the Lyapunov exponent which measures the asymptotic exponential rate of divergence of two initially infinitesimally close trajectories. The FSLE's application to dispersion in turbulent flow fields has been studied by Aurell and co-workers through numerical experiments on chaos and turbulence and particle tracking of a confined convective flow [1–6]. LaCasce and Ohlmann [7] used the FSLE to study relative dispersion at the surface of the Gulf of Mexico and Lacorata *et al.* [8] used it to study transport of balloons in the lower stratosphere and both found $\lambda_a(x) \sim x^{-2/3}$ for intermediate separations. The FSLE has also been applied in models of velocity structure to study stirring [9] and to discrete and continuous models having coupled fast and slow time scales [10,11].

As will become apparent, our definition of $T_a(x)$ and subsequent usage of the FSLE differs from earlier work. We explicitly include in the definition a way to account for flows where particles may get trapped in regions of space (e.g., eddies) where they continually resample separations. Additionally the FSLE has historically been defined as a discrete function of the initial separation. Our definition makes it a continuous function of initial separation which offers the possibility for more detailed theoretical study. Our goal is to provide a rigorous statistical mechanical definition for the a-time and employ this probabilistic approach in the FSLE to study dispersion during four disparate flow experiments. This expands the range of experiments for which the FSLE can be applied and additionally analyzes data differently by studying a variety of threshold ratios, a, rather than using a as a fixed parameter. The laboratory experiments include penetrative convection in a stratified fluid and steady flow in both heterogeneous and homogeneous porous media, while the numerical experiments involve one-dimensional deterministic diffusion and α-stable Lévy processes.

*Corresponding author. Email address: jcushman@purdue.edu

In the following subsections we introduce the systems that will be studied and place them in the context of their applicability. Section II details the statistical mechanical definition of the FSLE. Section III outlines the details of experimental setups. Section IV presents visualizations and FSLE results and the paper concludes in Sec. V.

A. Penetrative convection

The flux through the interface between a mixing layer and a stable layer plays a major role in understanding, characterizing and forecasting the quality of water in stratified lakes and the upper portion of the oceans and the quality of air in the atmosphere. The advance of a turbulent fluid into a fluid layer of stable stratification is called penetrative convection [12].

A penetrative convective flow is observed in the atmosphere when solar heating creates an unstable boundary layer at the earth surface. In many lakes an analogous phenomenon occurs starting from the upper free surface and penetrating downward with time. In the ocean, under calm conditions, the upper 20 or 30 m usually exhibit a continuous, moderately stable density distribution. When a wind begins to blow over the surface, turbulence in the water is generated both by the mean shear and by sporadically breaking waves. With elapsed time, entrainment or erosion by the turbulence of underlying denser water causes the turbulent layer to become deeper. Relatively rapid mixing creates an approximately uniform density distribution in the upper layer, and entrainment takes place across the interface between the turbulent and stable fluids [13].

When thermally induced, penetrative convection organizes into domes or spatial regions with significant vertical motion. The domes spring up from the heated surface below and stress the stable layer above creating internal waves above the mixing layer (in lakes and oceans domes emerge from the cooled surface above and stress the stable layer below). Convection is initially organized in persistent coherent structures, but later the flow becomes turbulent and the structures form and break randomly in space. Within the unstable layer, the fluid temperature, density and velocity change rapidly with time.

B. Porous media

Natural porous media can be found on scales that range from the nano (clays) to the global (lithosphere). Engineered porous media play a fundamental role in modern technologies such as drug delivery substrates, tile insulators, lubricants, and inkjet printers to name a few. Dispersion of chemicals in porous systems, which is important from both environmental and technological perspectives, is notoriously difficult to study experimentally. Although it is almost routine to image the internal structure of porous medium, it remains a great challenge to obtain trajectories of individual particles as they traverse the system.

Matched-index media which are transparent for a given wavelength of light offer great promise for studying Lagrangian flow fields in porous systems. The only naturally occurring matched-index medium is a cryolite-water mixture at room temperature; however, one can create an artificial liquid and solid matched-index system in several ways, one being a mixture of Pyrex and glycerol which is transparent to visible light at 23 °C. If a light scattering conservative tracer is introduced into such a system and a pressure gradient applied, then Lagrangian fluid-particle trajectories can be imaged within the pore space.

C. α-stable Lévy processes

α-stable Lévy processes are random processes which generalize Brownian processes by allowing for a larger variance for the process increments (the variance for the process itself is infinite). These processes have a variety of applications including microbial motility [14], anomalous dispersion [15], transport in fractal porous media [16], and turbulence theory [17]. A Lévy process can be utilized to model particle trajectories [14] or particle velocity [16].

For a each fixed time increment an α-stable Lévy process has an α-stable distribution [18]. We discuss here the one-dimensional case; however, it can be generalized to multidimensional setting. The α-stable Lévy process has stationary and independent increments. The parameters of the α-stable Lévy distribution, $S_\alpha(\sigma,\beta,\mu)$, are the index of stability $\alpha \leqslant 2$; the skewness β; the scale parameter σ; and the shift parameter μ. If $\alpha=2$, the distribution of the Lévy process at time t is a normal distribution, $N(2t\sigma,\mu)$, so a two-stable Lévy process is just a Brownian process. For $\alpha<2$ the second moment is infinite. The path created from the Lévy process is self-similar and fractal [19] with larger probability of long jumps for decreasing α. To simulate the Lévy process we utilize the well established Chambers-Mallows-Stuck code for an α-stable distribution [20].

There are several ways to obtain the FSLE from generated data. One can generate a reasonable amount of trajectories and then compare pairs of trajectories, reusing the trajectories at different starting points and hence different separations. Since this is a numerical experiment, more flexibility is allowed in the generation of trajectories. Alternatively, because the difference between two α-stable Lévy processes is also α-stable Lévy, one can generate a single trajectory and consider it as the difference of two trajectories. Both methods produce the same FSLE.

In general, the FSLE is a two-particle statistic but, as just pointed out, can sometimes be computed from a single-particle trajectory. If the distribution of the trajectories is known in advance (like the α-stable Lévy processes) and the distribution of the difference between trajectories is known, then it suffices to use a single trajectory. However, with experiments the distribution of the difference is not known a priori and so the FSLE must be computed using two particle statistics.

D. Deterministic diffusion

The Lagrangian map

$$x_{n+1} = x_n + p \sin 2\pi x_n \tag{1}$$

is well known to represent a deterministic diffusion [2]. We utilize this map to study issues of data analysis as well as to

examine the behavior of a well understood system. It also allows us to make comparisons with previous results on the FSLE.

II. THEORETICAL BACKGROUND

A. Finite-size Lyapunov exponent

Define $T_a(x)$ to be the average time required for two particles separated by a distance x to reach a distance ax apart for the first time. $T_2(x)$ is known as the doubling time and we call $T_a(x)$ the a-time. The aim is to embed T_a in a formal statistical mechanical framework and subsequently use it to define the FSLE.

Let $\Omega(t)$ denote the configuration pair space of dimension $N(N-1)d$, where d is the number of spatial dimensions needed to describe a particle position and N is the number of particles in the system. Consider the case where $d=3$. Points in $\Omega(t)$ are denoted by

$$(r_{1,2}(t),\theta_{1,2}(t),\Phi_{1,2}(t),r_{1,3}(t),\theta_{1,3}(t),$$
$$\times\Phi_{1,3}(t),\ldots,r_{N-1,N}(t),\theta_{N-1,N}(t),\Phi_{N-1,N}(t)).$$

The vector $(r_{ij}(t),\theta_{ij}(t),\Phi_{ij}(t))$ describes the separation between particles i and j in spherical coordinates where $r_{ij}(t)$ is the distance between the particles. In the definition of $T_a(x)$, only the radial coordinate is of interest and the others may be integrated away. Henceforth, without loss of generality, we let points in $\Omega(t)$ be represented by the radial degrees of freedom in $N(N-1)$-dimensional space.

Define the $N^2(N-1)^2$-dimensional pair separation space $\Omega(t,\tau)=\Omega(\tau)\times\Omega(t+\tau)$ which we endow with the probability measure f, where $f(r_{1,2}(\tau),r_{1,3}(\tau),\ldots,r_{N-1,N}(\tau),r'_{1,2}(t+\tau),r'_{1,3}(t+\tau),\ldots,r'_{N-1,N}(t+\tau))dr_{1,2}dr'_{1,2}\cdots dr_{N-1,N}dr'_{N-1,N}$ is the joint probability that particles i and j have separation in $(r_{i,j},r_{i,j}+dr_{i,j})$ at time τ and separation in $(r'_{i,j},r_{i,j}+dr'_{i,j})$ at time $t+\tau$, $\forall i=1,\ldots,N-1$, $j=1,\ldots,N$.

Let $G_\tau^{i,j}(x,y;\tau,t)$ be the conditional probability of two particles (i and j) being separated by a distance y for the first time at $\tau+t$, given they were separated by x at time τ. In the statistical mechanical framework outlined above, this can be written

$$G_\tau^{i,j}(x,y;\tau,t)=\frac{E[I_{A^{i,j}(\tau,t)}\delta(x-r_{i,j}(\tau))\,\delta(y-r_{i,j}(\tau+t))]}{E[I_{A^{i,j}(\tau,t)}\delta(x-r_{i,j}(\tau))]},\tag{2}$$

where $I_{A^{i,j}(\tau,t)}$ is the indicator function on the set

$$A^{i,j}(\tau,t)=\{r_{i,j}(\tau):e^{iLt'}r_{i,j}(\tau)<y\ \ \forall\ \ \tau\leqslant t'<\tau+t\},\tag{3}$$

ensuring that only the first time after τ that the particles reach the separation y is counted. Here δ is the usual Dirac delta distribution, the expectation is taken on the probability space (Ω,f) and L is the Liouville operator.

The integral

$$G^{i,j}(x,ax;t)=\lim_{\tau\to\infty}\frac{\int_0^\tau G_\tau^{i,j}(x,ax;\tau',t)d\tau'}{N_{x,y}^{i,j}(\tau,t)}\tag{4}$$

is the conditional probability that, given particles i and j are separated by a distance x at some time, they reach a distance y (for the first time) after t-time units have elapsed. $N_{x,y}^{i,j}(\tau,t)$ is the number of times that the particles i and j go from the distance x to y when the initial separation x occurs prior to time τ. The integration in Eq. (4) accounts for pairs of particles separated more than once by a distance x before time τ. For example, a pair of particles stuck in an eddy would periodically sample many separations. Each time a pair of particles reaches the distance x apart, τ acts as a new time origin. The denominator normalizes $G^{i,j}(x,ax;t)$. Since the limit of either the numerator or denominator may not exist, such as in a period flow, the limit must be taken after division. If a flow is to have a nonzero FSLE, then with probability one the particles must reach the desired threshold ax. Form the conditional probability for the system by averaging over all particles

$$G(x,ax;t)=\frac{1}{N(N-1)}\sum_{i\neq j}G^{i,j}(x,ax;t).\tag{5}$$

The a-time is the first moment of the probability defined in Eq. (5),

$$T_a(x)=E[G(x,ax;t)]=\int_0^\infty tG(x,ax;t)dt.\tag{6}$$

The statistical mechanical definition of the finite-size Lyapunov exponent is

$$\lambda_a(x)=\frac{1}{T_a(x)}\ln a\tag{7}$$

with $T_a(x)$ defined in Eq. (4). We refer to x as the initial separation and a as the threshold ratio.

This definition for the FSLE is greatly simplified in a system that is completely expansive, that is, when particles do not return to the initial separation x or to the threshold ratio y. In this case one can replace the definition of $G(x,y;t)$ with the simpler definition

$$G(x,y;t)=\frac{1}{N(N-1)}\times\int_0^\infty\sum_{i\neq j}\frac{E[\delta(x-r_{i,j}(\tau))\,\delta(y-r_{i,j}(\tau+t))]}{E[\delta(x-r_{i,j}(\tau))]}d\tau.\tag{8}$$

In this contribution, $G(x,ax;t)dt$ in Eq. (6) is calculated by discretizing time based on the size of initial separation and the type of system. To numerically confirm this is the average time of separation from x to ax, we have also calculated the a-time by pairwise averaging. The results of the methods agree for a variety of experiments, however, we emphasize that the definition in terms of probability densities is entirely mathematical in description. As all the experi-

ments yield data at discrete points, we have chosen to use linear interpolation between data points for analysis.

We expect that at the initial separations considered, all pairs of trajectories will have probability one of reaching the desired threshold in finite time, however, each experiment will have natural fluctuations in the a-time at any given separation. Since the data are from laboratory experiments, the trajectories are of different lengths and not all pairs of particles will achieve the desired separation ax in the time tracked. We maintained a record of the percent of pairs that reach the threshold in order to determine the accuracy of the FSLE for a given separation and threshold ratio. If the percentage of particles reaching the desired threshold is less than 100%, the a-time has been underestimated (the FSLE has been overestimated).

To handle the effect of the trajectory length, we made several comparisons and have imposed a fixed comparison time for analysis of an experiment. Two particles are compared only if there is at least the specified number of data points. Additionally, they are compared only for the specified amount of time even if more information is available. This prevents bias toward the shorter a-times in the data analysis as well as allowing us to uniformly cut off the upper times. This of course was not necessary for the deterministic diffusion and α-stable Lévy process.

III. EXPERIMENTAL SETTINGS

Particle tracking velocimetry (PTV) is a fully three-dimensional technique which allows one to determine trajectories by tracking individual particles. It is especially suited to a Lagrangian study of fluid motion, a feature that other techniques do not have [21]. The main steps in a PTV investigation are (i) seeding the flowing fluid with small highly reflecting particles; (ii) illuminating as uniformly as possible the flow field within a sampling window; (iii) acquiring images of the particles located within this window with an imaging rate that determines the time resolution of the method; (iv) preprocessing the images to eliminate background noise; and (v) determining the particle image coordinates in each frame with subpixel accuracy.

A. Matched-index porous media

In this experiment, three-dimensional (3D) trajectories are obtained inside porous media by stereoscopically matching orthogonal 2D projections. Details of the image analysis algorithms can be found in Moroni and Cushman [22]. Figure 1 illustrates the setup. Perspex boxes of dimensions $30\times30\times50$ cm^3 and $10\times10\times50$ cm^3 are used for test sections. These are filled with Pyrex pieces of varying size. Void space between the pieces is filled with glycerol, which at 23 °C has the same refractive index ($\sim$1.47) for visible light as for Pyrex. The glycerol is continuously circulated through the test section, top to bottom or bottom to top via a hydraulic circuit and a peristaltic pump. A high-power lamp lights the test section and two high-resolution cameras (2048×2048 pixels) with orthogonal optical axis record images (Fig. 1). To illuminate the medium and avoid the direct interaction among the light and cameras, a mirror has been used to create a light beam that moves with the draining fluid. Black frames were used to obtain square windows for observation.

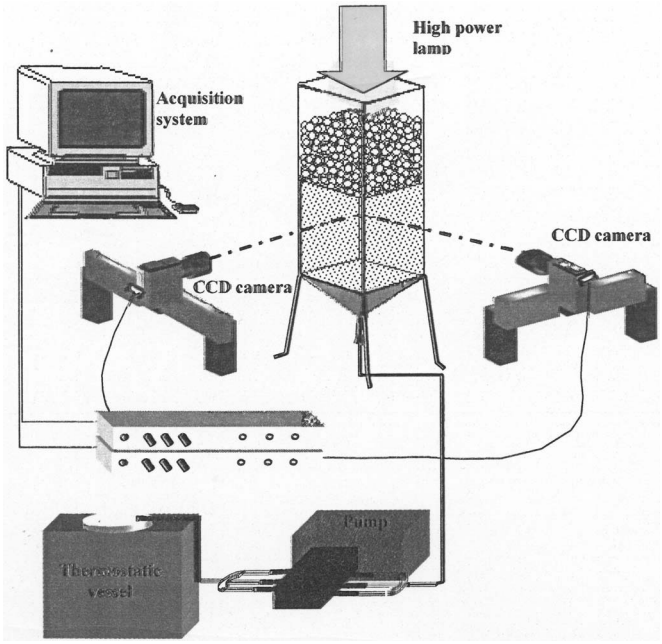

FIG. 1. Porous medium experimental setup.

A calibration system similar to that used in [22] is employed to minimize errors linked to image optical distortion and test-section acquisition-system misalignment. Accurate alignment of the camera acquisition system is critical to reducing errors caused by distortion of optical rays and accurate reconstruction of the third coordinate from two projected trajectories. A laser was used to align the system to check the camera optical axis horizontal angle and the test section walls vertical angle. The cameras, situated 1.8 m from the face of the test section, were coupled charge device (CCD) Kodak Megaplus 4.2 with an acquisition rate of one frame per second and resolution of 2048×2048 pixels.

The choice of tracers depends on the information one wants to gather. Since we are interested in passive mixing by a mean flow, the dimension of the tracer must be much smaller that the typical grain size. Generally one would want the specific weight of the tracer to be similar to the fluid, however since glycerol is highly viscous, we only need the viscous forces induced by fluid movement to dominate the buoyancy forces induced by the tracer particle. Because trajectories are obtained using an image analysis technique, the tracer must also be highly reflective to visible light. Air bubbles less than 0.1 mm diameter were chosen to satisfy these constraints.

A diffuser fed by a compressor was used to inject bubbles into the fluid. The diffuser was placed at the bottom of the container and embedded in 0.8 mm glass beads with the Pyrex particles placed above. When the compressor is turned on, the bubbles pass through the glass and into the Pyrex medium, distributing themselves in the void space. The lower square surface is screened and below the screen is an inverted pyramid shaped piece that connects the test section

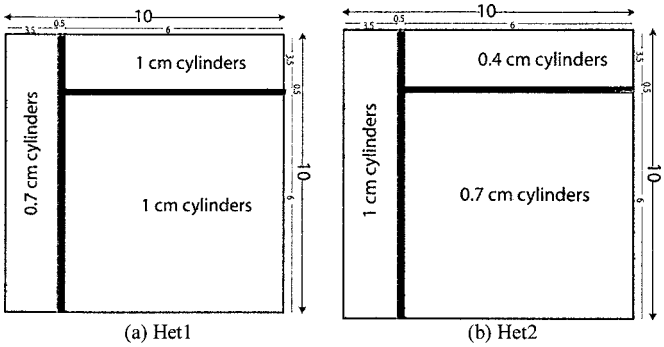

FIG. 2. Shaper and packing for the two heterogeneous media Het1 and Het2.

to the hydraulic circuit. The experiment begins when the peristaltic pump is turned on and the glycerol begins circulating through the test section. The air does not wet the solid, the bubbles are small (<0.1 mm) compared to the smallest grains (>0.4 cm) and due to the high viscosity of glycerol, the bubbles remain trapped in the fluid phase and flow passively with the draining fluid.

A homogeneous porous medium, Hom1, was constructed by placing 1.9 cm Pyrex spheres in the larger test section. The spheres were packed randomly but distributed homogeneously on the bench scale. To preserve the correct refractive index, they were carefully cleaned before being placed into the container. The average porosity was 42%. This medium was analyzed at three pumping speeds.

An additional homogeneous medium and two heterogeneous but periodic porous media were constructed in the smaller test section (Hom2, Het1, and Het2). Cylindrical particles of varying diameter were used: large (d=1 cm), medium (d=0.7 cm), and small (d=0.4 cm). A shaper (Fig. 2) was used to construct layers and each layer was rotated 90° from the layer immediately above and below. Though the figure shows three distinct regions in each layer, relaxation during packing created three amorphous sectors of roughly 5 cm height. A unit cell consists of four layers. Figure 2 illustrates the bead packing for the two heterogeneous media, Het1 and Het2, with average bead diameters 0.812 cm and 0.689 cm, respectively. The homogeneous medium for this

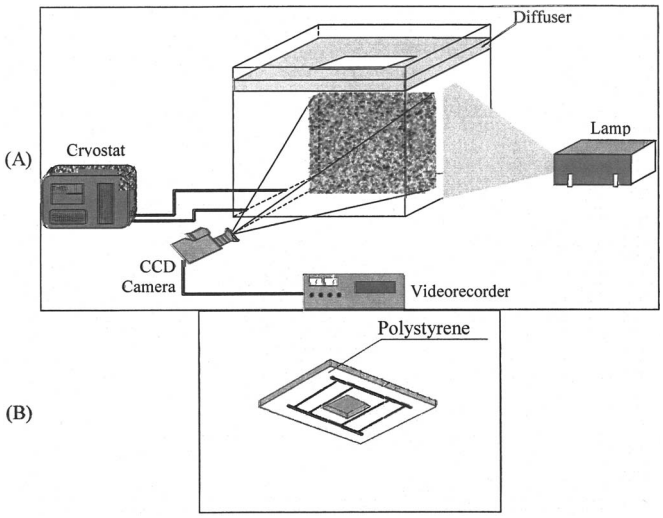

FIG. 3. Experimental setup (a) and water diffuser (b).

size test section was packed with 1-cm-diameter cylinders. These media are compared with the same pumping rate. Previous analysis has shown that Het2 and Hom2 behave similarly but differently than Het1 [22,23].

B. Penetrative convection

The laboratory model consists of a convection chamber containing an initially stable, density stratified fluid, which is heated from below causing destabilization. The bottom of the parallelepiped test section is horizontal and hence the fluid is homogeneous laterally. Heating the fluid from below creates penetrative convection. Distilled water is used for the fluid phase and fluoresceine is used to image the convective domes, i.e. the evolution of the mixing layer with time. Additionally, 80 μm pollen particles are used for the passive tracer to reconstruct particle trajectories. The test section is a tank with a square base (41×41 cm^2) and height 40 cm (Fig. 3). Its lateral sides are insulated by 3-cm-thick removable polystyrene sheets. When images are acquired, the insulation on the side facing the camera is removed. A diffuser, which also acts to insulate the upper surface, floats on the surface of the water as it initially fills the tank. A warm tank

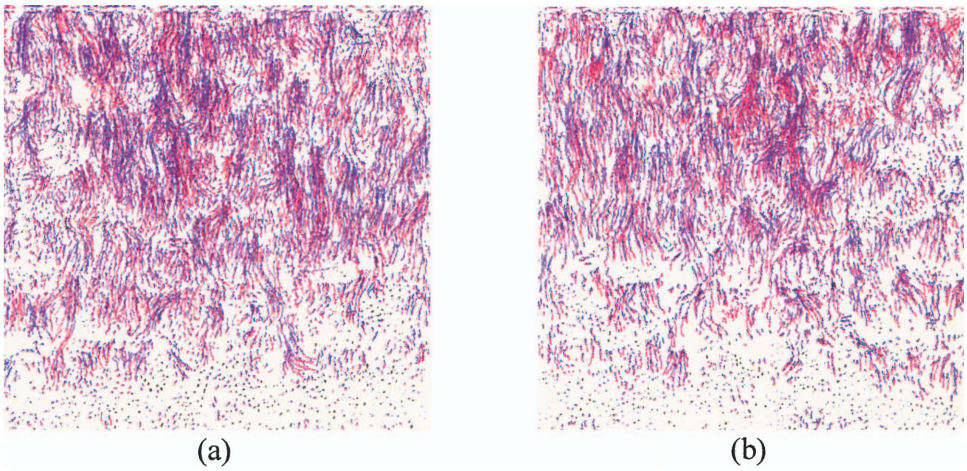

FIG. 4. (Color) Representative projections on the xz (left-hand side image) and yz planes (right-hand side image) of three-dimensional trajectories reconstructed through scanning 3D PTV for homogeneous media.

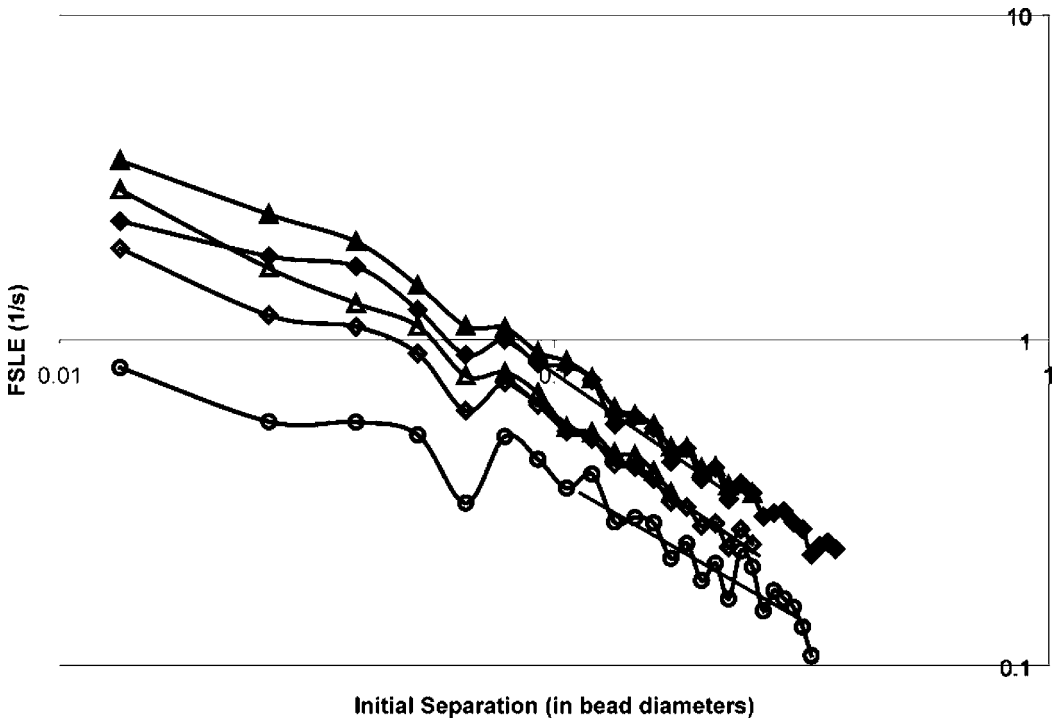

FIG. 5. FSLE for Hom1 for two velocities and two threshold ratios: slowest velocity results are the open markers $a=1.1$ (◯) 1.3 (◇), and 1.7 (△).

of water drains by gravity into a continually stirred colder tank and that tank in turn drains to the diffuser. While the diffuser floats upwards, it fills the test section creating a linear stratification of the fluid, cold to hot from bottom to top.

Thirty thermocouples were spaced vertically in the tank to record changes in temperature. Following initial stratification of the tank, a hot cryostatically controlled water bath was attached to a metal base plate and experiment begins. A 2-cm-wide light sheet was employed to illuminate the central region of the test section. Images of the pollen particles were recorded using a CCD camera with a time resolution of 25 frames per second.

The lower boundary was initially at temperature $T_0=288$ K and then rapidly increased to $T_m=292.6$ K. The initial temperature stratification was $\partial\bar{T}/\partial z=24$ K/m.

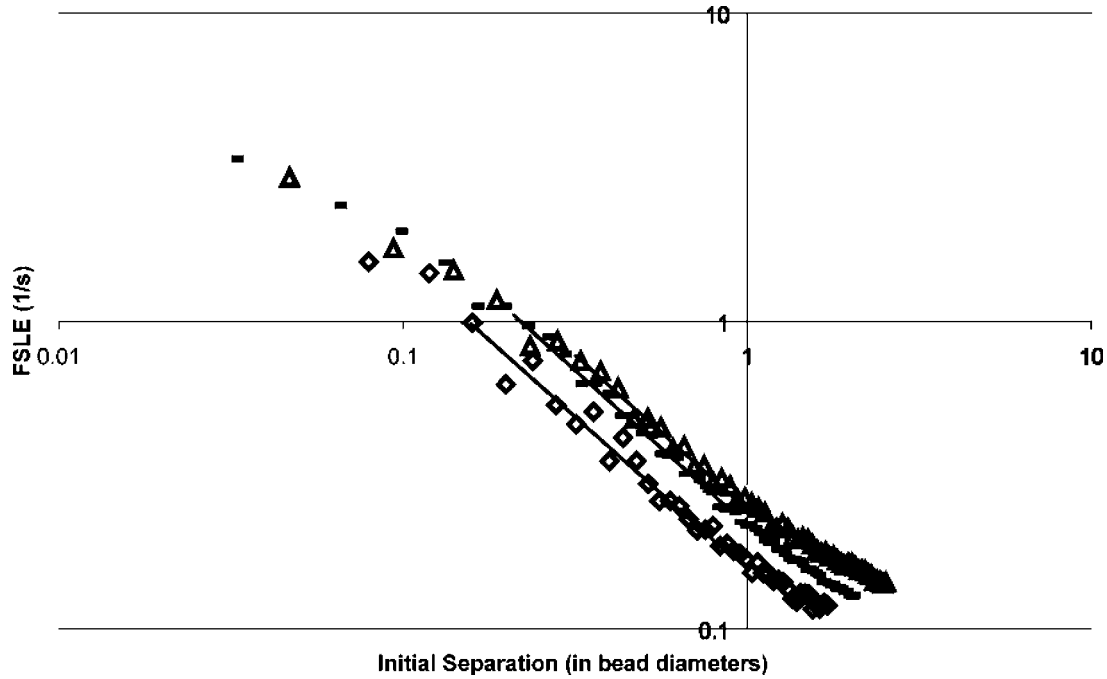

FIG. 6. FSLE for Het1 (◇), Het2 (△), and Hom2 (−). $a=1.6$.

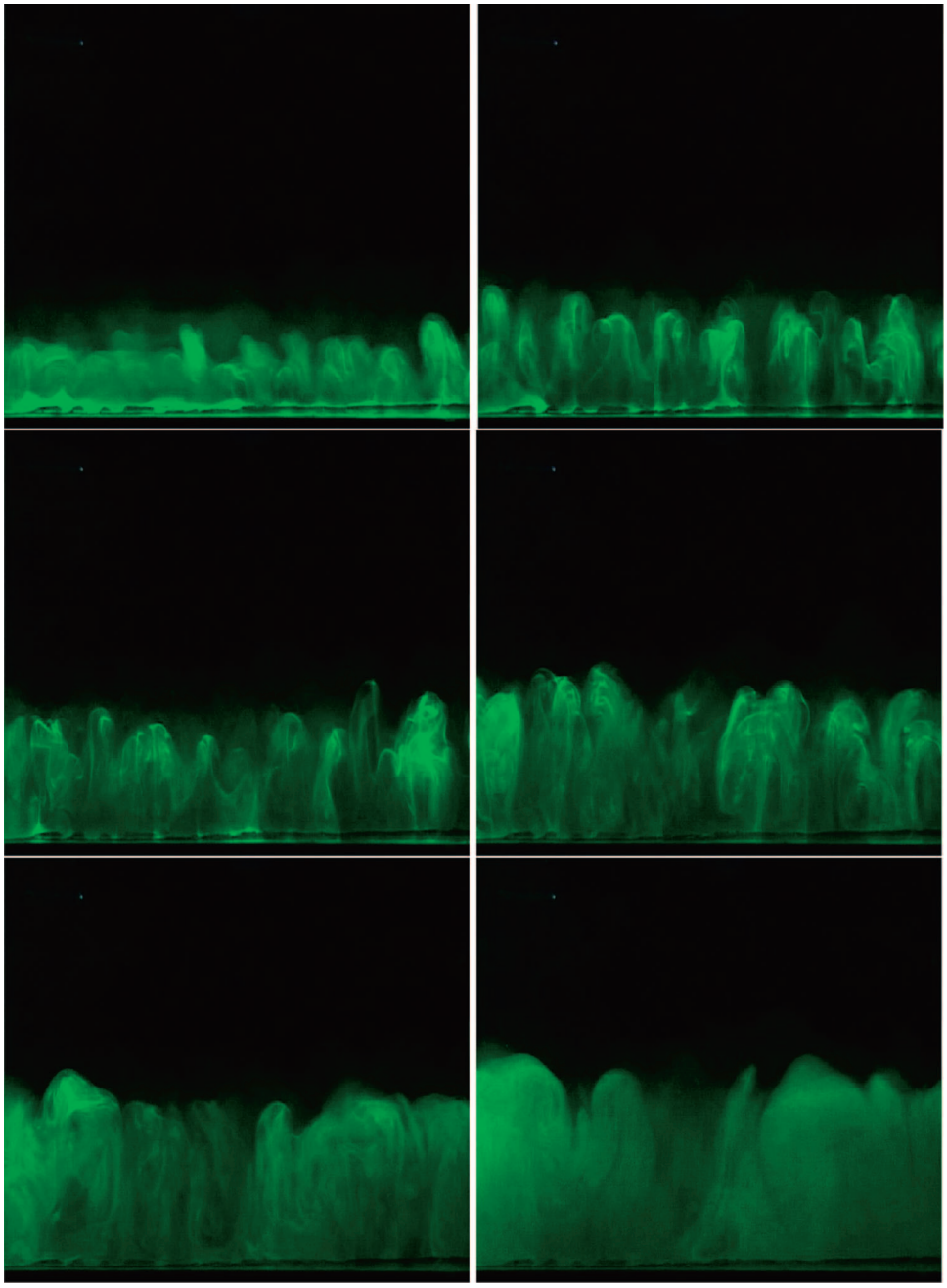

FIG. 7. (Color) Visualization of the mixing layer evolution.

IV. RESULTS

A. Porous media

Particle trajectories have been reconstructed using scanning 3D PTV and two projections are shown in Fig. 4. The two-dimensional trajectories prior to reconstruction have been analyzed in other contributions [22–24] to study the anomalous dispersive behavior the system exhibits.

All flows are initially non-Fickian; however, as time progresses they become Fickian in the direction of mean flow. For the homogeneous medium constructed with 1.9 cm spheres, increasing the velocity causes the system to transition to a Fickian regime faster. The higher velocity has larger longitudinal and transverse variances. In the smaller test section, Hom2 and Het2 both reach an asymptotic behavior, with Hom2 doing so sooner. Het1 does not transition to a Fickian regime in any direction during the life of the experiment.

The FSLE is a function of distance so the initial separation is normalized by the bead diameter. It was shown in [22] that for the larger test section, the tracer must cover three bead diameters to reach a Fickian regime in the transverse direction (depending on the pumping rate). For the other homogeneous medium, Hom2, the result is the same in the horizontal directions but in the longitudinal direction the tracer must cover about 13 bead diameters [23]. Since it is a two-particle statistic, the information the FSLE carries is substantially different than one particle statistics in generalized hydrodynamics studied by Moroni and Cushman [22,23,25].

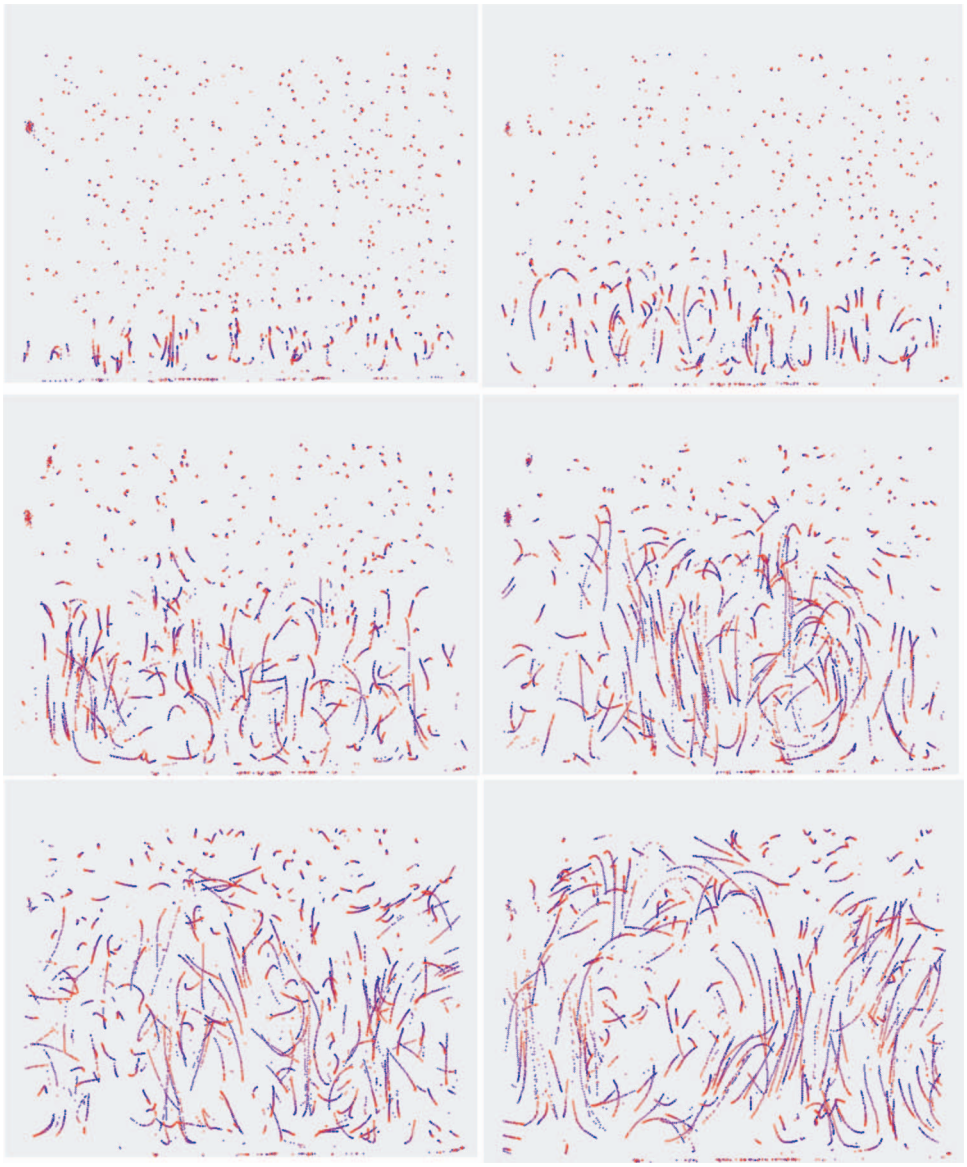

FIG. 8. (Color) Reconstructed centroids during mixing—color evolves from red to blue with time.

Figure 5 shows the FSLE for two different longitudinal velocities in Hom1 (0.36 and 0.54 cm/s). All trajectories employed in the analysis are followed for 10 s. Distance has been normalized to bead diameter and time is in seconds. The apparent scaling law is $\lambda_a(x) \sim x^{-\beta(a)}$ at the intermediate separations studied. The regions used for the least squares regression are indicated with a line of the appropriate slope. This is the region where the data are the most accurate. For the slowest velocity, $\beta(1.1) \approx 0.878$ and for $1.3 \leqslant a \leqslant 1.7$, $\beta = 1.05 \pm 0.02$. For the fastest velocity $\beta(1.1) \approx -0.86$, $\beta(1.3) \approx 1$ and requires a larger value of a to reach the exponent of 1.05 as seen from the data: $1.5 \leqslant a \leqslant 2$, $\beta = 1.05 \pm 0.03$. Since the higher velocity has shorter a-time, we are able to obtain data for larger a. For fixed a, higher velocity results in a faster rate of the separation as do larger threshold ratios. As the system goes Fickian, the FSLE should scale with x^{-2}, where x is the initial separation. However, we have not been able to compute the FSLE for threshold values or initial separations large enough to to test this scaling law.

As a approaches zero, the FSLE become horizontal. Aurell and co-workers point out that the FSLE converges to the classical Lyapunov exponent as x goes to zero for small enough a [1,4].

We have also explored the influence of trajectory length and found 10 s trajectories provide the best results for this experiment. The twelve smallest separations have 100% of the particles reaching the threshold, so there is no error in computing the FSLE. As x increases, the slope of the FSLE eventually decreases in magnitude. We believe this is a statistical artifact associated with the smaller number of trajectories reaching the a-time and have stopped the analysis prior to this event.

Figure 6 shows the FSLE for the smaller test section, again normalized by average bead diameter (presented in Sec. III A). The straight lines indicate the region where least squares regression was applied. For Hom2, $1.3 \leqslant a \leqslant 1.6$, $\beta = 1.05 \pm 0.01$, and Het2 $1.3 \leqslant a \leqslant 1.6$, $\beta = 1.01 \pm 0.01$. For Het1, $1.3 \leqslant a \leqslant 1.6$, $\beta = 0.98 \pm 0.01$. $\lambda_a(x)$ is largest for Het2 and smallest for Het1. This is demonstrated in the figure for $a = 1.6$, but also holds in general. The values of the FSLE increase with increasing longitudinal velocity, and longitudinal and horizontal variances. If the data is put in dimensional

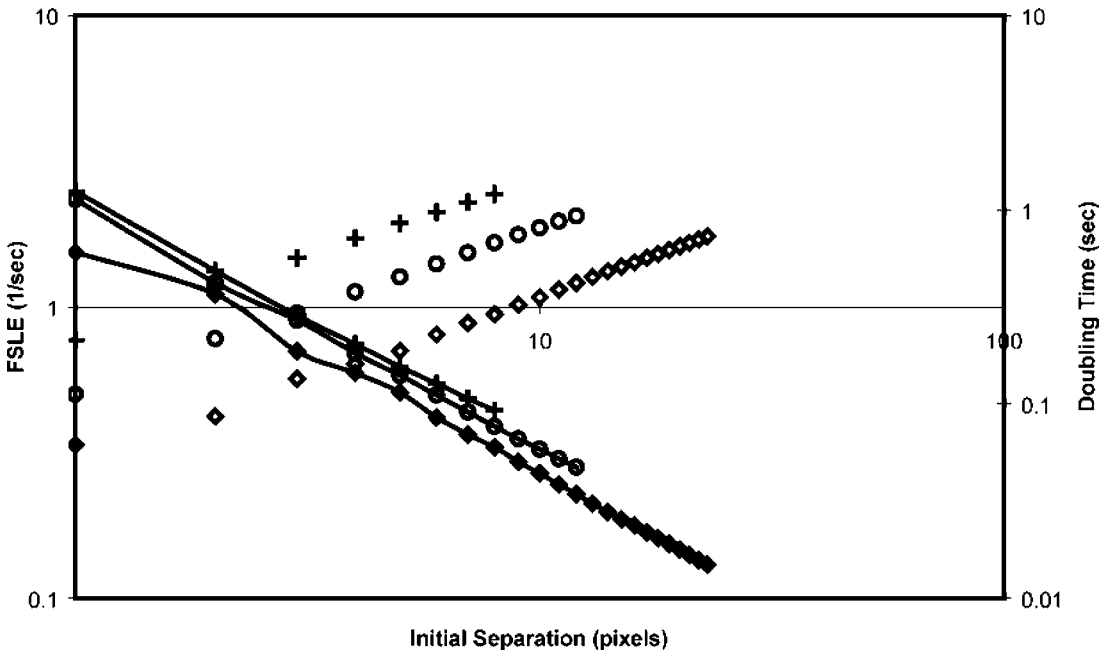

FIG. 9. The FSLE and the a-time for the mixing layer of penetrative convection for varying threshold ratios: $a=1.1$ ($\diamond$), 1.3 ($\bigcirc$), and 1.7(+). The points connected by a line are the FSLE (41 pixels=1 cm).

form, Hom2 has the fastest rate of separation. At least 99% of the particles are achieving the threshold for separations less than $\frac{1}{2}$ the bead diameter, giving a high quality estimation of the FSLE at these separations.

The FSLEs have been computed using the 2D data prior to construction of the 3D trajectories; however the FSLEs for the 2D and 3D trajectories are nearly identical when the percent of particles reaching the threshold is near 100%.

B. Penetrative convection

Typical images of the mixing layer are shown in Fig. 7; the image is of the central 2 cm of the test section. Domed structures and their growth with time are evident.

We introduce the Rayleigh number to describe the mixing layer behavior:

$$\mathrm{Ra} = \frac{\xi g \Delta T (z^*)^3}{\kappa \nu}$$

where ξ is the thermal expansion coefficient, κ the thermal diffusivity, ν the fluid kinematic viscosity, g the gravitational constant, and ΔT the temperature difference between the lower boundary and the top of the mixing layer of height z^*. κ is related to thermal conductivity k, the specific heat C_p, and density ρ by

$$\kappa = \frac{k}{C_p \rho}.$$

The onset of convection occurs when the Rayleigh number reaches a critical value. Ra increases with time because z^* increases. Low Ra convection is organized in coherent structures, but at higher Ra the flow becomes turbulent and the coherent structures (domes) appear and break continuously in space. Characteristic dimensions of the domes are the same order of magnitude as the mixing layer height, while their lifetime is generally less than the time a fluid particle needs to complete a revolution.

Three related structures occur over the life of the experiments: growing domes or turrets with an extremely sharp interface at their top, flat regions of rather large extent occurring after a dome or other structure has spread out or receded, and cusp-shaped regions of entrainment pointing into the convective fluid.

Particle tracking techniques are employed to reconstruct tracer particle trajectories inside the test section. Figure 8 displays barycenters reconstructed inside both the stable and the unstable layers as they evolve with time. In each panel, tracer particles and corresponding trajectories reconstructed over 50 consecutive frames are overlapped. The colors range from red to blue as a function of time.

Small line segments characterize particles with low velocity while long segments characterize fast particles. Fluid particles belonging to the mixing layer remain trapped within the layer. As the height of the mixing layer increases, particles belonging to the interface between the stable and unstable fluid begin oscillating along the transverse direction forming internal waves. Eventually the internal waves are entrained inside the mixing fluid.

Figure 9 shows the a-times and the FSLE for the mixing layer. The definition of the a-time is independent of the time origin and consequently the FSLE represents an average over the mixing layer as it grows. Three different threshold ratios a are shown. As discussed earlier, not all particles reach the desired threshold; we have chosen to cut-off the plots for initial separations when the percent of particles reaching ax falls below 75%. This cutoff was chosen to limit the underestimation of the FSLE while leaving enough data to study

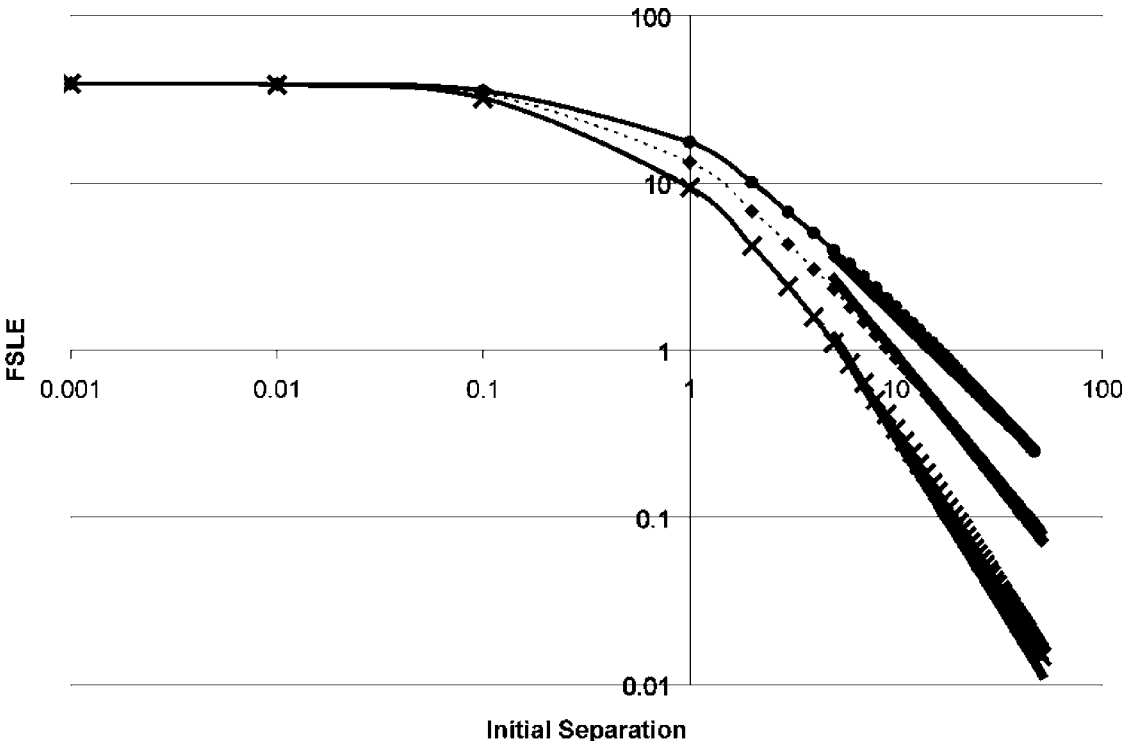

FIG. 10. FSLE for an α-stable Lévy process for three values of α (α=1.2, $\times$; 1.5, $\diamond$; 2, $\bullet$). Solid lines indicate the power law relation and have power equal to $-\alpha$.

the larger initial separations. Utilized trajectories were of length 2.6 s.

For these data, $\lambda_a(x) \sim x^{-\beta(a)}$ with $\beta \approx 0.86$ at $1.3 \leqslant a \leqslant 1.7$ for the intermediate separations studied. For smaller thresholds, β is smaller and for larger ratios the FSLE is larger. This means, for example, that there is a faster exponential growth rate for a set of particles with an average separation from x to $1.7x$ than from x to $1.1x$. A dependence on a is not surprising as increasing a causes the sampling of a larger range of movements in penetrative convection.

As a increases, so does the doubling time, hence the percent of particles reaching the threshold decreases. However, we note that the difference in this percentage at early separations for values $1.1 \leqslant a \leqslant 1.3$ is less than 1% and less than 2% when $1.1 \leqslant a \leqslant 1.7$. At nine pixels the graphs differ by 10% ($1.1 \leqslant a \leqslant 1.7$). The a-time reaches a maximum of 1.3 at these separations when the comparison time is 2.6 s. The decrease in percent of trajectories as a and x increase is most likely due to growing fluctuations in the a-time.

C. α-stable Lévy processes

Lévy processes were generated for several different index parameters, α where $\alpha > 1$ to guarantee a finite mean. The results are illustrated graphically in Figure 10. Plots are log-log and indicate a power law scaling in the initial separation for the asymptotic limit, $\lambda_a(x) = C_\alpha x^{-\alpha}$, where α is the index of stability. The results are for a fixed value of σ and $\beta = 0$. Utilizing least squares regression, the exponent was found to be $\alpha \pm 0.07$ for all values of α and a tested. Additionally we found a decreasing dependence of C_a on a as α decreased. The scaling relationship provides a quick and easy method to obtain α from a two particle statistic.

D. Deterministic diffusion

The deterministic diffusion data generated from Eq. (1) with $p = 0.8$ is examined to understand the effect a and x have on $\lambda_a(x)$. Our algorithm for computing $\lambda_a(x)$, as well as the definition of $\lambda_a(x)$, differs from that of Aurell and co-workers [1–6]. However, for time stationary data, such as the deterministic diffusion data, our definition will coincide with previous definitions. We present several different values of the FSLE for various threshold ratios (Fig. 11). As a increases, the FSLE decreases. The relative difference between $\lambda_{1.1}(x)$ and $\lambda_{1.6}(x)$, $[\lambda_{1.1}(x) - \lambda_{1.6}(x)]/\lambda_{1.1}(x)$ remains near 35% after the system goes asymptotic. In all cases, at least 99% of the trajectory pairs reach ax. We note that we have used a linear interpolation between points of the deterministic diffusion rather than simply taking the first unit time the separation is beyond the threshold. This makes the a-time smaller; hence $\lambda_a(x)$ is slightly larger than the results presented in [2].

The irregularities in the intermediate region highlight the sensitivity to the code parameters. Since a probability density is being calculated, one must use a discretized time. For shorter doubling times (smaller x and smaller a) a finer mesh must be utilized. The results in Fig. 11 correspond to a fine discretization for x less than 6 (number of bins per time increment is 15), and a coarser disrecretization for $x > 6$ (number of bins per time increment is 5). We used the coarse mesh on the intermediate separations to show the effect of the bin size, which is minor fluctuations in the FSLE.

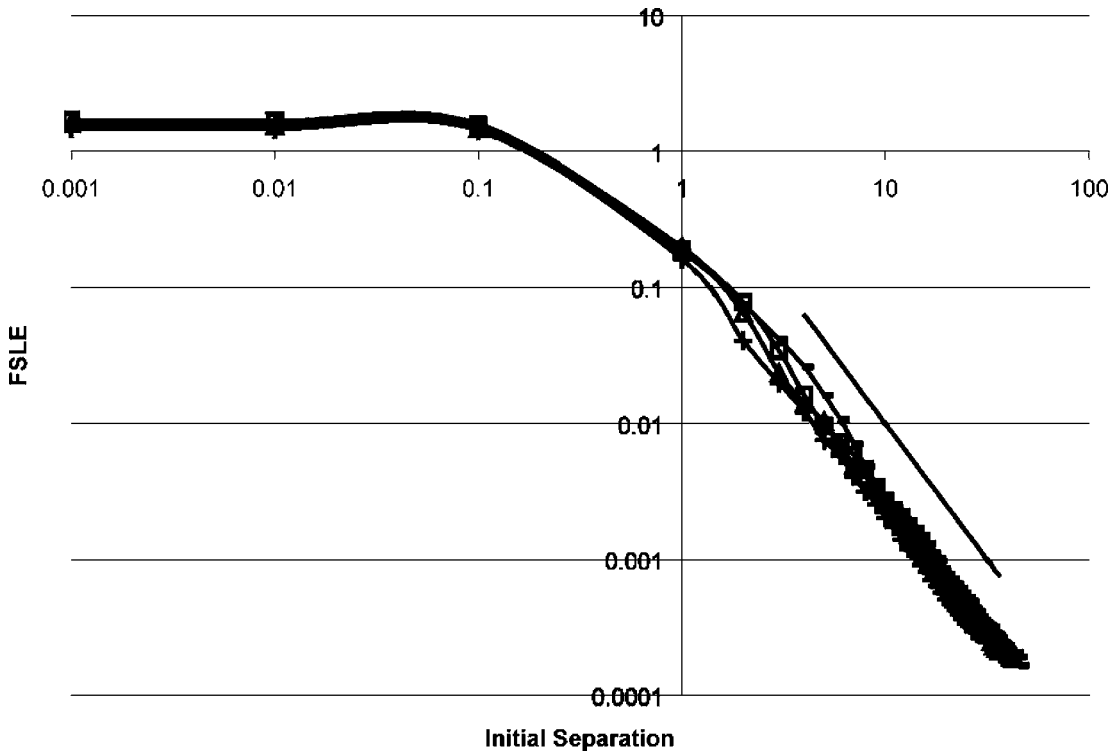

FIG. 11. FSLE for deterministic diffusion: solid line shows slope of −2; $a=1.1(-)$, 1.2 (□), 1.3 (△), and 1.6(+).

Least squares regression was performed on this data and the exponent was between 1.98 and 2.

V. CONCLUSIONS

A rigorous statistical mechanical definition of the FSLE has been presented. The definition of the a-time explicitly takes into account such phenomena as recirculation, nonstationary systems and periodic processes as well as providing a solid mathematical definition for the FSLE.

The probabilistic definition for the FSLE has been applied in several experiments. We analyzed the behavior of the FSLE, $\lambda_a(x)$, for four systems: penetrative convection, flow in porous media, Lévy processes, and deterministic diffusion. In each experiment, for intermediate initial separations x, the apparent scaling relation is $\lambda_a(x) \sim x^{-\beta}$. The exponent β is dependent on a in the pre-Fickian laboratory experiments, however the dependence of β on a decreases with increasing a. There is no dependence of β on a for the Lévy motion or deterministic diffusion. The coefficient of proportionality depends on a for all systems.

For the homogeneous porous media, the value for β increases with increasing a, up to $\beta \approx 1.05$. The decreasing dependence of β on a, as a increases, is associated with the evolving heterogeneity in the preasymptotic regime. Increasing the velocity increases the FSLE and the higher velocity did require a larger a to attain $\beta \approx 1.05$. The most heterogeneous medium (Het1) had a lower β than the homogeneous media at all threshold ratios. Het2 in many ways behaves as a homogeneous medium [23,24], but has a β value between Hom2 and Het1.

The penetrative convection experiment had a lower β and hence has a slower growth rate of the a-time with initial separation than the porous media. It also had β increasing with a; however, this rate of growth slowed as a increased. As was the case for all the porous media experiments, the FSLE increases with increasing a. This interesting phenomena is opposite to the deterministic diffusion data and Lévy process and is clearly associated with the physics of the preasymptotic regime. Recall that both the penetrative convection and porous media experiments are preasymptotic, while the deterministic diffusion and Lévy processes are not.

For the α-stable Lévy processes, the relationship $\lambda_a(x) \sim C_a x^{-\alpha}$ holds with the dependence on a entirely in the coefficient of proportionality. This important result gives a quick method to determine the stability parameter α from data that display a Lévy behavior such as flagellated microbes [14]. The deterministic diffusion map was used to verify the asymptotic behavior $\lambda_a(x) \sim x^{-2}$ and also fits well with the results from the α-stable Lévy process. The deterministic diffusion is a deterministic model for a two-stable Lévy process. It was shown that increasing a caused a decrease in $\lambda_a(x)$, but the exponent remained unchanged. The effect of a decreases with decreasing α for Lévy processes.

The results presented here differ from previous work in several important ways and begin to extend the definition of the FSLE for use beyond stationary systems, such as penetrative convection where all separations times from x to ax are counted for $T_a(x)$. Earlier studies had the threshold ratio fixed and small to prevent sampling over many scales of experiment. In this work, the ability to see the effect of the scale by varying the threshold ratio is seen as an important component in the study of the growth rate of the mixing zone at different scales of observation. By varying both a and x we can better observe the growth of the mixing zone over multiple scales.

ACKNOWLEDGMENTS

The authors would like to thank Professor Antonio Cenedese who is responsible for the laboratory where experiments and image analysis were performed. The work reported herein has been sponsored by the National Science Foundation under Contracts No. 0310029-EAR and No. 0417555-EAR. N.K. would also like to thank Purdue Research Foundation.

[1] E. Aurell *et al.*, Phys. Rev. Lett. **77**, 1262 (1996).
[2] E. Aurell *et al.*, J. Phys. A **30**, 1 (1997).
[3] V. Artale *et al.*, Phys. Fluids **9**, 3162 (1997).
[4] G. Boffetta, M. Cencini, S. Espa, and G. Querzoli, Phys. Fluids **12**, 3160 (2000).
[5] G. Boffetta *et al.*, Chaos **10**, 50 (2000).
[6] G. Boffetta, M. Cencini, S. Espa, and G. Querzoli, Europhys. Lett. **48**, 629 (1999).
[7] J. H. LaCasce and C. Ohlmann, J. Mar. Res. **61**, 285 (2003).
[8] G. Lacorata E. Aurell, B. Legras, and A. Vulpiani, J. Atmos. Sci. **61**, 2936 (2004).
[9] F. d'Ovidio, V. Fernández, E. Hernández-García, and C. López, Geophys. Res. Lett. **31**, L17203 (2004).
[10] G. Boffetta, A. Crisanti, F. Paparella, and A. Provenzale, Physica D **116**, 301 (1998).
[11] G. Boffetta, P. Giuliani, G. Paladin, and A. Vulpiani, J. Atmos. Res, **55**, 3409 (1998).
[12] J. W. Deardorff, G. E. Willis, and D. K. Lilly, J. Fluid Mech. **35**, 7 (1969).
[13] H. Kato and O. M. Phillips, J. Fluid Mech. **37**, 643 (1969).
[14] H. C. Berg, Phys. Today **53** (1), 24 (2000).
[15] M. M. Meerschaert, D. A. Benson, and B. Bauemer, Phys. Rev. E **59**, 5026 (1999).
[16] M. Park, N. Kleinfelter, and J. H. Cushman, preceding paper, Phys. Rev. E **72**, 056305 (2005).
[17] J. H. Cushman, M. Park, N. Kleinfelter, and M. Moroni, Geophys. Res. Lett. **32**, L19816 (2005).
[18] G. Samorodnitsky and M. S. Taqqu, *Stable Non-Gaussian Random Processes: Stochastic Models with Infinite Variance* (Chapman and Hall, New York, 1994).
[19] K. Falconer, *Fractal Geometry: Mathematical Foundations and Applications*, 2nd ed. (Wiley, New York, 2003).
[20] A. Janicki and A. Weron, *Simulation and Chaotic Behavior of α-Stable Stochastic Processes* (Marcel Dekker, New York, 1994).
[21] M. Virant and T. Dracos, Meas. Sci. Technol. **8**, 1539 (1997).
[22] M. Moroni and J. H. Cushman, Phys. Fluids **13**, 81 (2001).
[23] M. Moroni, J. H. Cushman, and A. Cenedese, Int. J. Eng. Sci., **41**, 337 (2003).
[24] M. Moroni, N. Kleinfelter, and J. H. Cushman (unpublished).
[25] J. H. Cushman and M. Moroni, Phys. Fluids **13**, 75 (2001).